Iridescent anthophyllite-gedrite from Simiuttat, Nuuk district, southern West Greenland: composition, exsolution, age

K. A. RODGERS

Department of Geology, University of Auckland, Private Bag 92019, Auckland, New Zealand

P. D. KINNY

Department of Applied Physics, Curtin University of Technology, GPO Box U1987 Perth, Western Australia 6001

V. R. MCGREGOR

Atamnik, DK-3912 Maniitsoq, Greenland, Denmark

G. R. CLARK

Department of Chemistry, University of Auckland, Private Bag 92019, Auckland, New Zealand

AND

G. S. HENDERSON

Department of Geology, University of Toronto, 22 Russell Street, Toronto, Ontario M5S 3B1, Canada

Abstract

Golden iridescent, <1–100 mm crystals of alternating lamellae of anthophyllite and gedrite constitute the bulk of orthoamphibolite pods within quartz-cordierite gneisses of the Akulleq terrane at Simiuttat, SW Greenland. X-ray powder diffraction powder gave a = 18.526(7), b = 17.979(15), c = 5.285(23) Å; a single crystal has a = 18.546(7), b = 17.950(16), c = 5.280(1) Å, space group P_{nma} with some reflections being notably broader than others. Spot EMPA yielded composite analyses: Al^{IV} = 0.89–1.3, $Mg/(Mg+Fe^{2+})$ = 0.57–0.61, Na/Al^{IV} = 0.22–0.26. AFM imaging of {210} cleavage surfaces, showed a uniform corrugated morphology parallel to [001]; wavelength was 190–350 nm, mean 250 nm, amplitude 3 nm. A plan view resembles TEM images of (010)-parallel exsolution textures of orthoamphiboles. A second set of corrugations may crosscut the [001]-parallel ridges at 20–25°, akin to reported lamellar intergrowths developed parallel to both (010) and (120). Unequivocal evidence linking topography with lamellae is absent. In contrast to the conventional multi-layer reflector model, the ridged surface provides an additional origin for iridescence, acting as a diffraction grating. Included zircons, 50–10 μm, have Hf/Zr = 0.008–0.012, $Hf+Fe^{II}$ *c.* 0.16. $^{207}Pb/^{206}Pb$ ages are from 2690 to 2770 Ma, averaging 2732 ± 10 Ma. Coexisting, included Th-, La-, Ce-, Pr-, Nd-, Gd-, Y-monazites have $^{207}Pb/^{206}Pb$ ages from 2680 to 2720 Ma, averaging 2707 ± 12 Ma. The included crystals grew during a late Archaean metamorphism that produced overgrowths on zircons within gneisses to the north, but with Simiuttat grains showing a more complex history. The lamellae may have developed at the same time, or during a reheating *c.* 2550 Ma, or in a subsequent Proterozoic metamorphism.

KEYWORDS: anthophyllite, gedrite, cell parameters, composition, iridescence, lamellae, age, nuummite.

Introduction and geological setting

NEAR monomineralic rocks composed of iridescent orthoamphiboles have been found at several localities in the Nuuk district of southern West Greenland. All the occurrences lie within a well-defined stratigraphic unit of supracrustal rocks dominated by quartz-cordierite gneisses, that is up to 100 m thick

Mineralogical Magazine, December 1996, Vol. 60, pp. 937–947

and which can be traced discontinuously along strike for tens of kilometres (Beech and Chadwick, 1980; Dymek and Smith, 1990; McGregor *et al.*, 1991; Smith *et al.*, 1992; McGregor, 1993). This unit is within the Akulleq terrane, a NE–SW-trending belt of rocks with very varied lithologies that range in age from 3870 to 2820 Ma. The Akulleq terrane is interpreted as an accretionary complex formed by stacking crustal slices of different types and ages at the margin of a late Archaean continental mass, with syntectonic intrusion of granitic *(s.l.)* magmas into the pile (McGregor *et al.*, 1991; McGregor, 1993). During terrane assembly in the late Archaean, the quartz-cordierite gneisses and associated rocks were subjected to very intense, planar, ductile deformation. All lithological units have become strongly attenuated with many, including the iridescent orthoamphibole rocks, reduced to strings of disconnected lenses. Slip along lithological boundaries has largely destroyed original stratigraphic relationships.

Rocks with iridescent orthoamphibole are also known from near Kangerluarsuk in the Maniitsoq district, 150 km north of Nuuk, in a different geological setting. Selected samples from both settings are used locally as semi-precious gemstones under the trade name 'Nuummite'.

A general account of unlocated examples of Nuuk iridescent amphiboles was given by Appel and Jensen (1987). A more rigorous description is given here, confined to an occurrence on the north coast of the middle, large island of Simiuttat, 45 km south of Nuuk, lat. 63° 47.0'N, long. 51° 39.4'W, in the Akulleq terrane (Beech and Chadwick, 1980; McGregor *et al.*, 1986). At this locality the orthoamphibole rock occurs as a lens, some 3 metres thick, enclosed in a unit of quartz-garnet, dark grey amphibole rock several metres thick. This unit in turn occurs within a sequence tens of metres thick of pale bluish-grey quartz-cordierite gneisses. The massive, dark green-black to dark grey, iridescent amphibole rocks consist principally of anthophyllitic-gedritic orthoamphibole crystals <1 mm to 100 mm in size, associated with minor amounts of other silicates and patchy sulphide mineralization. No evidence is seen of reaction zones.

This paper gives a detailed mineralogical description of the orthoamphibole rock including AFM examination of the iridescent surfaces, as well as estimates of the timing of amphibole growth and exsolution based on SHRIMP-derived ages of included zircon and monazite.

Mineralogy

The present Simiuttat samples (University of Auckland, Department of Geology, mineral collection AU3296-3299; Australian Museum collection D49914)) are coarse-grained, xenomorphic-granular rocks, consisting primarily of elongate, anhedral to subhedral orthoamphibole with minor pyroxene, biotite, narrow blades of ilmenite, local clusters of feldspar, and rare quartz and xenotime. Individual amphibole crystals range from a few to fifteen millimetres in length and poikilitically enclose infrequent, small, 10–100 μm, round crystals of zircon and irregular-shaped monazite grains up to 500 μm in size. Pyrrhotite, pyrite, chalcopyrite and magnetite are present.

Orthoamphibole

X-ray powder diffraction of a bulk Simiuttat sample, using a Philips diffraction goniometer fitted with a graphite monochromator and employing Cu-$K\alpha$ radiation, yielded a well developed orthoamphibole pattern along with low intensity reflections corresponding to major diffraction lines of orthochrysotile, esseneite, orthopyroxene (near hypersthene), sanidine-like alkali-feldspar, quartz and pyrrhotite.

Cell dimensions for the orthoamphibole derived from least squares refinement of thirty-seven reflections indexed in the diffraction pattern of the concentrate (Table 1), are a = 18.526(7), b = 17.979(15), c = 5.285(23) Å. Indices of most reflections correspond to those of Seki and Yamasaki (1957) and Milton and Ito (1961). Traces of quartz in the sample were used as an internal standard.

Single crystal diffraction analysis of one pale golden iridescent crystal gave a = 18.546(7), b = 17.950(16), c = 5.280(1) Å, with all diffraction spots being satisfactorily indexed on a single orthorhombic cell, space group P_{nma}. Some reflections were noticeably broader than others and $2\theta/\omega$ and ω scans were performed to analyse spot profiles. A few reflections were found where the broad spots had separated into two. A second gedrite crystal was mounted to further check this phenomenon. The same unit cell was produced, and again some reflections appeared broader than others. Further scans were performed but no spots were found that had separated into two — the broad reflections were just broad. There was no correlation between broad or doubled spots on the first crystal with broad spots on the second. Hence we deduced that any broadening or splitting is an artefact of a particular crystal, rather than an inherent property of the crystal lattice of this sample of gedrite (*cf.* Treloar and Putnis, 1982).

The orthoamphibole powder pattern also showed a broadening and/or a broad skewing of some diffraction lines such as might be expected from the association of two closely similar phases in

TABLE 1. X-ray powder diffraction data for orthoamphibole, Simiuttat

d(Å)	I/I_o	*hkl*	d(Å)	I/I_o	*hkl*	d(Å)	I/I_o	*hkl*
8.98	18	020	2.834	13	251	2.026	4	532
8.23	37	210	2.743	20	630	1.996	7	612
5.05	5	230	2.707	4	531	1.981	10	062
4.62	3	400	2.680	13	351	1.977	6	751
4.50	7	040	2.585	14	161	1.973	4	670
4.115	19	420	2.544	9	202	1.872	4	702
3.870	4	131	2.502	11	451	1.830	7	722
3.644	10	231	2.429	5	302	1.772	10	10.30
3.331	8	331	2.343	5	650	1.735	9	491
3.225	37	440	2.314	5	800	1.665	2	323
3.043	100	610	2.151	8	660	1.624	2	902
3.006	9	431	2.133	13	561			
2.872	12	521	2.064	6	821			

Note: 1. Relative intensities are affected by preferred orientation
2. a = 18.526(7), b = 17.979(15), c = 5.2853(23)

subequal amounts but it was not possible to translate this broadening into differing unit cell dimensions.

Iridescence: The iridescent sheen of Nuuk anthophyllite-gedrite was the first reported example of the effect in amphiboles, with Bøggild (1905, 1924) relating it to included lamellae oriented parallel to (010). More recently, Appel and Jensen (1987) ascribed the effect in the Nuuk crystals to internal reflections off alternating gedrite and anthophyllite exsolution lamellae, as had been documented for similar orthoamphiboles (e.g. Gittos *et al.*, 1976; Robinson *et al.*, 1971; Ghose, 1981; Robinson *et al.*, 1982).

An editorial note appended to Appel and Jensen's paper (1987, p.42) characterized the Nuuk iridescence as having "a spangled pattern associated with aventuresence. Each 'spangle' or bright reflection is reminiscent of labradoresence". Appel and Jensen note that the number of iridescent grains varies from one or two per cm^2 to dozens per cm^2 and described a variety of iridescent types among polished samples ranging from green and metallic blue through yellow to golden-red with rare violet. Smaller grains typically show a variety of colours while larger crystals tend towards golden and reddish shades. Very large grains show little or no iridescence.

The present Simiuttat samples have body colour ranging from BCC 226 Charcoal Grey to BCC 230 Howard Green. Crystals up to 15 mm long display a dominant iridescence ranging from BCC 66 Buff through BCC 67 Almond Shell to BCC 75 Chartreuse Yellow, all suffused with BCC 74 Golden Brown. Other colours evident on unpolished cleavages of grains of similar size, and dependant on orientation, include BCC 43 Alice Blue, BCC 44 Steel Blue grading to BCC 73 Mace, with rare BCC 76 Green Muscat. The green-blue, green-red, blue-gold, red, red-gold and purple colours reported by Appel and Jensen (1987) are absent from the present samples. True opaline colours occur in crystal fractures within feldspar clusters.

Composition: The small size of the Simiuttat orthoamphibole lamellae precludes their individual analysis by standard electron microprobe techniques with *c.* 3 μm beam diameter and only composite analyses were obtained. Some four dozen spots of the principal Simiuttat amphibole were analysed using a JEOL JXA-5A instrument operating at an accelerating voltage of 15 kV and an adsorbed sample current of *c.* 650 pA, with a Link Systems LZ-5 EDS detector. Raw data were corrected using a QX 2000 processor and ZAF-4/FLS quantification software version QX 20-24F-1291. Spot traverses from core to rim indicate that each crystal is relatively homogeneous, but overall there is a slight variation between crystals. Three representative analyses that span the compositional range encountered are given in Table 2.

Structural formulae were calculated on a basis of 23(O) using the method of Droop (1987) to distribute total Fe between Fe^{2+} and Fe^{3+}. Total tetrahedral Si+Al was constrained to 8. The remaining cations available for M_1, M_2, M_3 and M_4 sites totalled near 7 in all cases prior to normalisation of total cations to 15. Only in analysis 1 of Table 2 was the total sufficiently above 7 to require more than 0.1% total iron to be calculated as Fe_2O_3. Compositions plot within the gedrite field and extend into anthophyllite

TABLE 2. Electron microprobe analyses of orthoamphibole, Simiuttat

	1	2	3		1a	2a	3a
SiO_2	49.41	48.72	47.02	Si	7.108	7.019	6.838
TiO_2	0.14	0.1	0.23	Al^{IV}	0.892	0.981	1.162
Al_2O_3	8.55	10.09	11.27	Al^{VI}	0.560	0.732	0.769
Fe_2O_3	0.32	–	<0.1	Ti	0.015	0.003	0.025
FeO	21.38	20.04	19.64	Fe_3	0.034	–	<0.005
MnO	0.18	<0.1	<0.1	Fe_2	2.572	2.414	2.388
MgO	17.32	17.52	17.11	Mn	0.022	–	–
CaO	0.52	0.42	0.45	Mg	3.714	3.763	3.710
Na_2O	0.80	0.84	1.08	Ca	0.080	0.065	0.070
K_2O	n.d.	n.d.	n.d	Na	0.222	0.234	0.304
F	0.10	<0.1	0.21	F	0.046	–	0.096
Subtotal	98.72	97.81	97.07	A/Al^{IV}	0.25	0.23	0.26
F=O	0.04	–	0.09	X_{Mg}	0.59	0.61	0.61
Total	98.68	97.81	96.98				

1, 2, 3: wt% oxides; n.d. = not detected; 1a, 2a, 3a: structural formulae on basis of 23(O); Fe^{3+} and Fe_2O_3 estimated after Droop (1987)

as defined by the IMA (Leake, 1978): Al^{IV} ranges from 0.89 to 1.3, $Mg/(Mg+Fe^{2+})$ is limited to between 0.57 and 0.61, and Na/Al^{IV} is restricted from 0.22 to 0.26.

AFM imaging: A Digital Instruments Nanoscope III Atomic Force Microscope (AFM) was used to examine the {210} cleavages from several iridescent crystals. Cleavage fragments were imaged in distilled water using standard Si_3N_4 pyramidal tips mounted on 200 μm-wide legged cantilevers. Contact forces were estimated at ⩽20 nN. The D scan head (12.5 μm × 12.5 μm), operating in either constant height or constant force mode, was used for all images and was calibrated against a gold standard. A range of scan rates and scan directions were used.

All images were fully reproducible. Each shows a corrugated morphology in which ridges and furrows extend uniformly across the {210} cleavage surface with a more or less consistent width and spacing. While not strictly linear, the corrugations are near parallel to [001]. Bifurcation is common, with some corrugations seemingly attenuating in points. Wavelength varies from 190 to 350 nm (Fig. 1*a*) with an amplitude of 3 nm. The corrugations shown in Fig. 1*b* have wavelengths ranging from 194–342 nm with a mean of 256 nm and a mode of 210 nm, noting that AFM measurements have an error of ±20% due to tip convolution effects. Tip convolution during a traverse can also obfuscate the shape of a ridge-furrow cross-section, with squared or angular ridge edges being imaged as a curve, and may also contribute to the irregular, somewhat subglobular aspect of corrugations seen at high magnifications (Fig. 1*d*).

The plan view of the AFM imaged surface shows distinct similarities with TEM images of exsolution textures of orthoamphiboles (e.g. Ghose, 1981, Figs 23, 24; Smelik and Veblen, 1993, Fig. 1.). The common exsolution lamellae oriented parallel to (010) are typically long compared with their finite width. Interfaces are seldom perfectly straight but show a roughly uniform width and spacing. Branching is common, with lamellae displaying tapering, pointed terminations. Individual lamellae commonly range up to and may exceed 200 nm thickness as a result of coarsening, following initial nucleation. These coincidences in plan texture between AFM and TEM images find further correspondence in AFM images where a series of deeper set lineations with a wavelength *c.* 250 nm crosscut the common [001]-parallel ridges at angles of 20–25° (Fig. 1*c*). Smelik and Veblen (1993, Figs 5,6) describe a similar orthoamphibole texture arising from an association of lamellar intergrowths developed parallel to both (0$\bar{1}$0) and (120). A corrugation wavelength of 210 nm on the (210) surface would correspond to a gedrite/anthophyllite pair lamella thickness of *c.* 190 nm along [010], placing the Simiuttat images towards the coarser end of the typical orthoamphibole range although not at its extreme (Robinson *et al.*, 1971; Smelik and Veblen, 1993).

The limitations of AFM technology frustrate elucidation of the true nature of the corrugated topography. Structural details are lacking that might provide unequivocal evidence that the imaged topography is an expression upon the cleavage

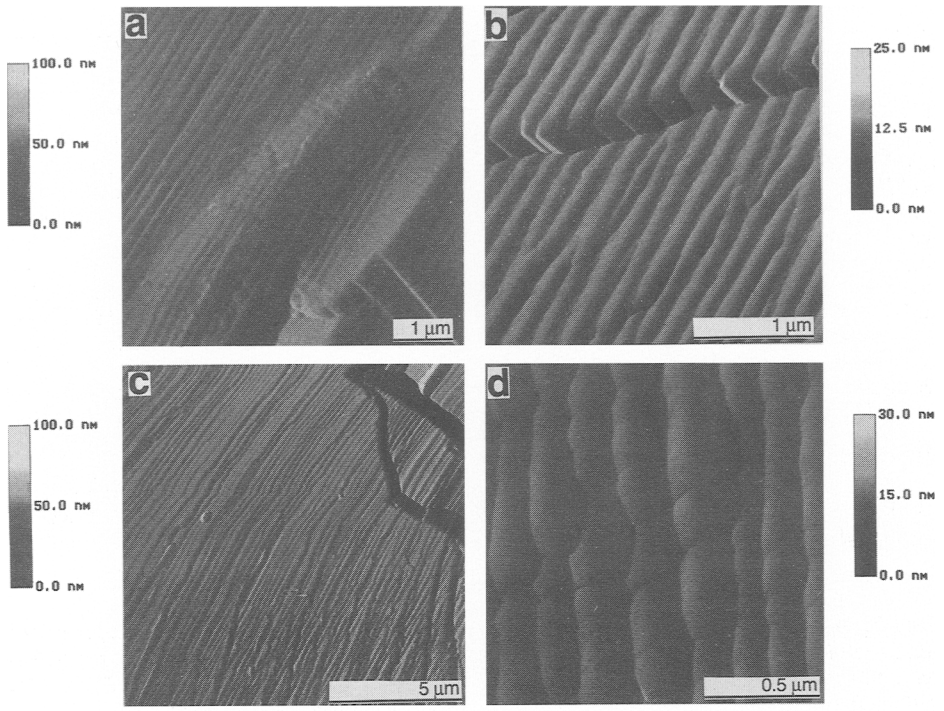

FIG. 1. Atomic Force Microscope images of {210} cleavages from golden iridescent orthoamphibole crystal. (*a*) Typical, corrugated, [001]-parallel, morphology, extending uniformly across and lengthwise along well developed {210} cleavage surface and intersected by pinacoidal cleavages. Scan size 5.184 µm, imaged in water. (*b*) Corrugations developed near parallel to [001] bifurcate and attenuate as tapering points, while continuous across a pinacoidal cleavage step. The vertical depth from crest of one ridge to trough of an adjacent furrow, in mid-field, is about 3 nm. Scan size 2.831 µm, imaged in water. (*c*) Corrugated, [001]-parallel ridged topography, crosscut at an angle of 20–25° by a second set of deeper corrugations some 250 nm wide. Scan size 13.00 µm, imaged in air. (*d*) Enhanced magnification image that suggests the corrugations are somewhat irregularly developed along their length, having a subglobular appearance. Care needs to be exercised in making such an interpretation as the appearance may be no more than an artifact arising from tip convolution. Scan size 1.486 µm, imaged in water.

surface of the underlying lamellae. Irrespective of the validity of such an interpretation, intriguingly, the ridged and furrowed surface possesses the attributes of a diffraction grating and consequentially provides an additional source for the iridescence of natural cleavages (cf. Parker, 1995). A ridge periodicity near 200 nm is consistent with a yellow iridescence, as is a similar spacing of lamellae pairs in the conventional multi-layer reflector model of Robinson *et al.* (1971). Colour variation seen in differing orientations as observed among Simiuttat orthamphiboles is readily explicable in terms of a grating. Little or no variation is necessary in the spacing of the diffracting ridges. Colour variation could be restricted if a blazed grating exists. However, in the absence of TEM or similar studies of these Simiuttat lamellae, the precise relationship between underlying structure, topography, and lamellae remains ambiguous.

Zircon

Composition: The orthoamphibole encloses small (50 × 100 µm), scattered, pale mauve, visibly zoned, subhedral grains of zircon. Electron microprobe spot analyses of several grains were made using an ARL SEMQ wavelength dispersive instrument operating at an accelerating voltage of 15 kV and an adsorbed sample current of *c.* 0.015 µA. Spot size was *c.* 3 µm.

TABLE 3. Electron microprobe analyses of zircons and monazite included in Simiuttat orthoamphibole, Greenland

	1	2	3		1a	2a
SiO_2	32.53	32.48	0.61	Si	3.840	4.016
ZrO_2	65.12	63.37	n.d.	Zr	3.748	3.820
HfO_2	0.94	1.41	n.d.	Hf	0.032	0.048
ThO_2	<0.1	0.13	0.87	Th	–	0.004
La_2O_3	n.d.	n.d.	9.76	La	–	–
Ce_2O_3	<0.1	n.d.	24.69	Ce	–	–
Pr_2O_3	n.d.	n.d.	4.80	Pr	–	–
Nd_2O_3	<0.1	<0.1	12.92	Nd	–	–
Sm_2O_3	n.d.	n.d.	4.21	Sm	–	–
Gd_2O_3	n.d.	n.d	3.89	Gd	–	–
Y_2O_3	<0.1	0.21	4.39	Y	–	0.012
FeO*	1.43	1.09	–	Fe*	0.140	0.112
MgO	<0.1	0.10	–	Mg	–	0.020
CaO	<0.1	<0.1	0.56	Ca	–	–
K_2O	n.d.	<0.1	–	K	–	–
P_2O_5	0.23	0.18	29.09	P	0.004	0.020
Total	100.67	99.16	95.79			

1, 2, 1a, 2a: zircons; 3: partial analysis of monazite; 1, 2, 3: wt.% oxides; 1a, 2a: structural formulae on basis of 16(O); * = total iron as FeO (or Fe^{II}); n.d. = not detected

Raw data were corrected using $\phi(\rho z)$ software of Armstrong (1988). Analyses showed a range of SiO_2 30.48–32.53, ZrO_2 62.42–65.12, HfO_2 0.93–1.41, ThO_2 0.1–0.44, and FeO* 1.05–1.43, with Hf/Zr ratio 0.008–0.012, and the sum $Hf+Fe^{II}$ consistently near 0.16 e.g. Table 3, columns 1,2. Most analyses showed notable phosphorus and yttrium. The zircons luminesced very poorly under cathodoluminescence, but showed contrast in zonation under backscattered electron imaging.

Age: Twenty grains were dated using the SHRIMP II ion microprobe at the Western Australia Isotope Science Research Centre, Perth (Table 4). One 25 μm diameter site was analysed per grain. A primary O_2^- beam current of 1.5 nA was used, and a mass resolution of *c.* 4500R, leading to a detection sensitivity for Pb isotopes of 15 counts per second per ppm. Subtraction of common Pb, which was modelled on the composition of Broken Hill ore Pb, was based on the measured ^{204}Pb. $^{206}Pb/^{204}Pb$ ratios were upwards of 10000. Pb/U ratios were corrected for instrumental inter-element fractionation by normalization to the Perth standard zircon CZ3 ($^{206}Pb^*/^{238}U = 0.0914$; 564 Ma). With one exception, U contents of the analysed sites ranged from 300 to 1100 ppm, Th from 2 to 13 ppm, Th/U ratios $\leqslant 0.022$. The exceptional analysis, grain 6, is lower in U (200 ppm) and higher in Th (31 ppm).

On a Wetherill concordia diagram the analyses form a group overlapping concordia with a mean $^{207}Pb/^{206}Pb$ age of 2732 ± 10 Ma (Fig. 2). The data are, however, scattered beyond the expected analytical uncertainty, the overall range in $^{207}Pb/^{206}Pb$ ages being from 2690 to 2770 Ma. The exceptional grain 6 is discordant and distinctly older, with a minimum $^{207}Pb/^{206}Pb$ age of 2862 ± 24 Ma.

Monazite

Composition: Small, irregular shaped crystals of monazite occur throughout the specimens examined, larger in size (up to 500 μm) but less abundant than the coexisting zircon inclusions. Electron microprobe analysis of three grains gave consistent results, using a three-spectrometer Cameca Microbeam instrument with $\theta = 90°$ and $\phi = 40°$, operating at an accelerating voltage of 15 kV, a beam current of 38 nA, and a total analysis time of 420 s. The electron spot was slightly defocused to minimize decomposition of the monazite and a weak green-blue cathodoluminescence permitted beam focussing. All oxides for which standards were available were determined and showed ranges of ThO_2 0.77–0.87, Y_2O_3 4.23–4.26, La_2O_3 9.67–9.77, Ce_2O_3 22.46–24.69, Pr_2O_3 4.47–4.80, Nd_2O_3 11.98–12.92, Sm_2O_3 3.95–4.21. In all cases totals proved low and

TABLE 4. SHRIMP U–Pb isotopic analytical data for mineral inclusions in orthoamphibole rock, Simiuttat, West Greeland

Grain Spot	U	Th	Pb	Th/U	$^{206}Pb/^{204}Pb$	%c206	$^{206}Pb/^{238}U$	±1σ	$^{207}Pb/^{235}U$	±1σ	$^{207}Pb/^{206}Pb$	±1σ	$^{207}Pb/^{206}Pb$ Age	±1σ
Zircon														
6.1	203	31	115	0.154	11040	0.145	0.5222	0.0107	14.72	0.33	0.2045	0.0015	2862	12
3.1	985	2	532	0.003	33320	0.048	0.5247	0.0105	13.96	0.29	0.1930	0.0006	2767	5
4.1	881	8	461	0.009	32460	0.049	0.5088	0.0102	13.46	0.28	0.1919	0.0006	2758	6
18.1	542	10	287	0.018	27510	0.058	0.5146	0.0103	13.58	0.29	0.1914	0.0008	2754	7
16.1	928	4	514	0.004	13080	0.122	0.5393	0.0108	14.19	0.29	0.1908	0.0006	2749	6
1.1	682	2	367	0.004	29735	0.054	0.5240	0.0105	13.78	0.29	0.1907	0.0008	2748	7
8.1	1001	7	545	0.007	19410	0.082	0.5305	0.0106	13.82	0.29	0.1890	0.0006	2734	5
19.1	1103	4	615	0.003	23310	0.069	0.5445	0.0109	14.18	0.29	0.1889	0.0006	2732	5
15.1	772	8	429	0.010	8685	0.184	0.5398	0.0108	14.04	0.29	0.1887	0.0007	2730	6
14.1	475	9	250	0.018	13150	0.122	0.5118	0.0103	13.30	0.28	0.1885	0.0009	2729	8
7.1	919	13	528	0.014	24020	0.067	0.5594	0.0112	14.53	0.30	0.1883	0.0006	2728	5
10.1	536	9	288	0.017	21350	0.075	0.5238	0.0105	13.57	0.29	0.1879	0.0008	2723	7
17.1	299	6	159	0.020	20410	0.078	0.5169	0.0105	13.38	0.29	0.1877	0.0011	2723	10
9.1	458	10	247	0.021	12350	0.129	0.5235	0.0106	13.53	0.29	0.1874	0.0009	2719	8
20.1	865	9	470	0.011	11540	0.139	0.5294	0.0106	13.64	0.28	0.1869	0.0007	2715	6
5.1	758	7	398	0.009	29860	0.054	0.5129	0.0103	13.18	0.27	0.1864	0.0007	2711	6
13.1	477	9	255	0.018	15620	0.102	0.5208	0.0105	13.37	0.28	0.1862	0.0009	2709	8
12.1	509	9	263	0.018	10520	0.152	0.5031	0.0101	12.88	0.27	0.1857	0.0009	2704	8
2.1	362	8	190	0.022	17840	0.090	0.5112	0.0104	13.04	0.28	0.1850	0.0011	2698	9
11.1	409	8	213	0.019	17660	0.091	0.5080	0.0103	12.88	0.28	0.1839	0.0010	2689	9
Monazite														
2.5	1930	6800	1870	4	151800	0.011	0.5470	0.0079	14.12	0.21	0.1873	0.0002	2718	2
1.2	1060	18800	2620	18	35130	0.046	0.5507	0.0080	14.19	0.21	0.1869	0.0002	2715	2
2.3	2220	4500	1880	2	118800	0.013	0.5515	0.0080	14.20	0.21	0.1867	0.0002	2713	2
1.3	550	12200	1560	22	29090	0.055	0.5169	0.0075	13.27	0.20	0.1862	0.0003	2709	3
1.4	700	23100	2740	33	16530	0.097	0.5251	0.0076	13.47	0.20	0.1860	0.0003	2707	3
2.6	230	10300	1330	45	19780	0.081	0.5289	0.0077	13.55	0.21	0.1859	0.0005	2706	5
1.5	3000	9600	2690	3	117900	0.014	0.5210	0.0076	13.34	0.19	0.1857	0.0001	2704	2
1.1	600	11000	1580	18	17920	0.089	0.5288	0.0077	13.53	0.20	0.1856	0.0003	2703	3
1.8	520	8500	1280	16	18450	0.087	0.5398	0.0078	13.76	0.20	0.1849	0.0003	2697	3
1.7	650	10400	1540	16	15330	0.104	0.5152	0.0075	13.12	0.19	0.1848	0.0003	2696	3
(.6	740	11300	1650	15	23055	0.069	0.5180	0.0075	13.17	0.19	0.1844	0.0003	2693	3
2.1	260	9700	1280	37	13225	0.121	0.5259	0.0076	13.35	0.20	0.1841	0.0005	2690	4
2.2	700	10500	1620	15	30550	0.052	0.5357	0.0078	13.54	0.20	0.1833	0.0003	2683	3
2.4	560	8900	1070	16	12830	0.125	0.4594	0.0067	11.03	0.16	0.1742	0.0004	2598	4

Isotope ratios refer to radiogenic Pb. %c206 is the percentage of common ^{206}Pb, as determined using the measured ^{204}Pb.
U, Tb and Pb concentrations are in ppm

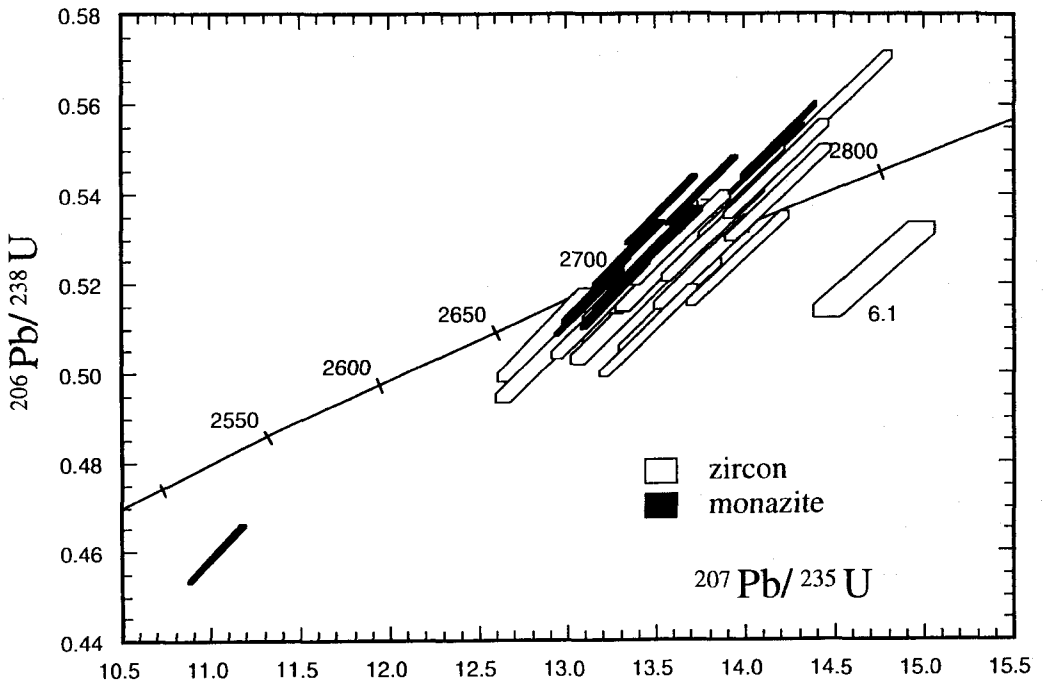

FIG. 2. Concordia plot for zircon and monazite analyses of Table 3. One sigma error boxes corresponding to individual SHRIMP spot analyses are shown. The zircon data (shown in white) cluster about a mean $^{207}Pb/^{206}Pb$ age of 2732 ± 10 Ma but are too scattered to represent an undisturbed single-age population. Grain 6, with a minimum age of 2862 ± 24 Ma, is distinctly older. The monazite data (in black) form a narrower cluster with $^{207}Pb/^{206}Pb$ ages ranging from 2680 to 2720 Ma, and a mean value of 2707 ± 12 Ma.

analyses with the JEOL JXA-5A instrument using the virtual standards package of the LINK Analytical ZAF-4/FLS software indicated the presence of small amounts of heavy rare earth elements.

Age: Two 100 μm × 3–500 μm monazite inclusions were dated using the Perth SHRIMP, with a total of fourteen 25 μm sites being analysed. A primary O_2^- beam current of 2.0 nA was used, and a mass resolution of *c.* 4500R, leading to a detection sensitivity for Pb isotopes of 70 counts per second per ppm. Common Pb correction procedures were as for zircon, with $^{206}Pb/^{204}Pb$ ratios > 10000 once excess background interference peculiar to monazite analysis was subtracted from the ^{204}Pb peak. Pb/U ratios were normalised using the 'MAD' monazite standard ($^{206}Pb^*/^{238}U = 0.0829$; 513 Ma).

The analysed monazites show a similar, but more restricted range in isotopic composition than the zircons (Table 4, Fig. 2). With the exception of one discordant analysis (# 2.4), $^{207}Pb/^{206}Pb$ ages ranged from 2680 to 2720 Ma, with a mean value of 2707 ± 12 Ma. Most analyses overlap concordia, a few are marginally reverse discordant.

Discussion

Petrologic evolution: The very siliceous host quartz-cordierite gneisses have very unusual compositions, being enriched in magnesium, iron and aluminium, depleted in calcium, sodium and potassium and strongly enriched in incompatible trace elements such as zirconium, hafnium and niobium. They have been interpreted by Dymek and Smith (1990) and Smith *et al.* (1992) as derived from felsic volcanoclastic sediments that were hydrothermally altered by heated seawater, the volcanic sources having affinities with A-type (anorogenic) granites. Smith *et al.* (1992) suggest that the associated amphibolites were derived from basaltic material intercalated within the felsic volcanoclastic sediments and that the massive orthoamphibole rocks were produced by diffusive

interaction between amphibolite pods and the host quartz-cordierite gneiss during regional metamorphism. There is no evidence to support such an origin at the locality where the samples discussed in this paper were collected. The orthoamphibole rock here occurs as a pod in quartz-cordierite gneisses and is not closely associated with the amphibolite.

Age relationships: It is useful to compare the zircon inclusion ages for the present Simiuttat orthoamphibole rock with SHRIMP ages obtained from zircons in quartz-cordierite gneiss on the southern tip of Sallersua Island, 6 km north of Simiuttat (sample PK10, reported by Friend *et al.*, in press). The quartz-cordierite gneiss zircons from Sallersua are larger than those in the orthoamphibole rock studied here and are composed of distinct cores and rims. The cores yielded a concordant mean age of 2833 ± 6 Ma, their uniform composition and age supporting the idea of a (hydrothermally altered) felsic volcanic or volcaniclastic source for the precursor of the gneiss as proposed by Dymek and Smith (1990) and Smith *et al.* (1992). The rims were more varied in composition, and were characterised by a distinctly lower Th/U ratio (0.01 to 0.1) than the enclosed cores (0.2 to 1.1). They yielded a mean age of *c.* 2717 Ma with excess scatter of the data points beyond the expected analytical uncertainty and, given their very low Th/U, were interpreted as having grown under amphibolite facies metamorphic conditions (*cf* Williams and Claesson, 1987; Maas *et al.*, 1992), possibly in competition with a Th-rich phase such as monazite.

The main Simiuttat zircon population (this study) yielded a similar range in Th/U and apparent age to the Sallersua zircon rims (Fig. 3). We therefore interpret them as having grown during the same late Archaean metamorphic episode. The same interpretation is also applied to the Simiuttat monazites dated here, which gave ages overlapping those given by the zircons (Fig. 3). During the same time interval, numerous granite sheets and diatexites formed in the Akulleq and adjoining terranes. It has been suggested that tectonic crustal thickening occurred in the region at this time, when the Akulleq terrane was overridden by the Tasiusarsuaq terrane from the south, and that this was accompanied by moderate to high pressure metamorphism along a clockwise $P-T-t$ path (Nutman *et al.*, 1989). The fact that both the Sallersua zircon rims and the present Simiuttat zircons and monazites yielded a significant spread in $^{207}Pb/^{206}Pb$ apparent ages from *c.* 2750 to 2690 Ma could be taken to indicate a protracted period of elevated $P-T$ conditions or alternatively a series of closely spaced metamorphic peaks within this time interval. It is possible that early formed monazites recrystallized during later stages of metamorphism, which would explain why the monazite ages group towards the lower end of this interval (Fig. 3). The overall spread in zircon ages could be a Pb loss phenomenon.

Most of the tiny zircon inclusions in the Simiuttat orthoamphibole rock appear to have grown entirely *in situ*. Only one older core was found in twenty analysed grains. Its minimum age of 2862 ± 24 Ma is

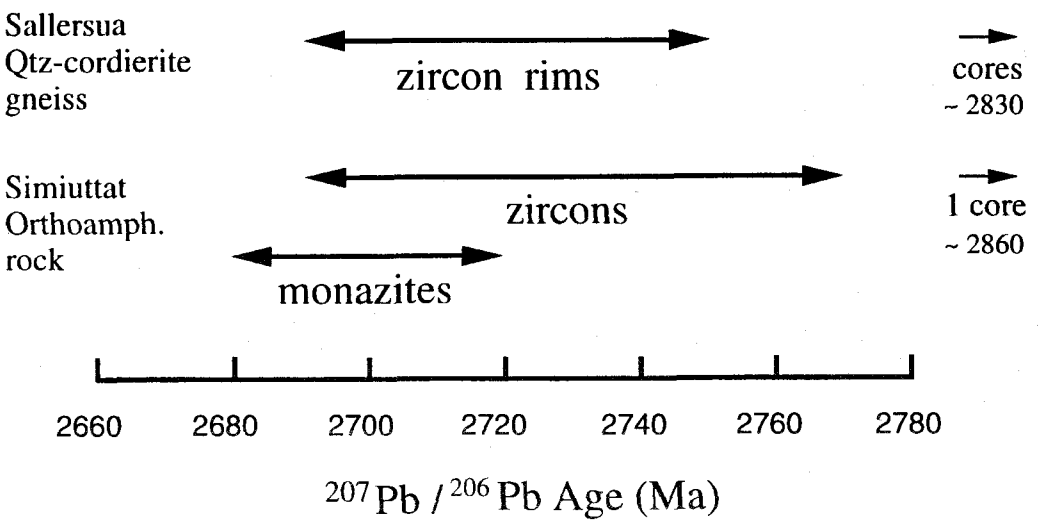

FIG. 3. Summary of SHRIMP age data for zircon and monazite inclusions in the Simiuttat orthoamphibole rock, as compared with zircon data from quartz-cordierite gneiss on nearby Sallersua (PK10).

marginally older than the mean age of the Sallersua quartz-cordierite gneiss zircon cores suggesting a possibly different source, but more analyses would be required to confirm this. Whatever the source, it can be concluded that unlike the quartz-cordierite gneiss, detrital zircons constituted only a relatively minor component in the precursor to the orthoamphibolite rock, and that the majority of zircon and monazite grains formed from the breakdown of other minerals during amphibolite facies metamorphism.

The most likely time for crystallization of the orthoamphibole is during this period of deformation and amphibolite facies metamorphism between *c.* 2750 and 2680 Ma, as recorded by the zircon and monazite inclusions. However, amphibolite facies conditions associated with further deformation in the region, perhaps at lower pressures, were reached again at *c.* 2550 Ma, the time of intrusion of the Qôrqut sheeted granite complex in a linear belt extending to within *c.* 5 km of Simiuttat (McGregor *et al.,* 1991). Additional weaker thermal activity *c.* 1550 to 1770 Ma is indicated by Rb-Sr mica ages from early Archaean gneisses of the Akulleq terrane (Pankhurst *et al.,* 1973; Baadsgaard *et al.,* 1976), however extensive recrystallisation did not take place during this period since late Archaean mineral ages *c.* 2500 Ma are preserved in other isotopic systems (K-Ar hornblendes, U-Th-Pb in titanite, apatite and allanite).

Origin of the lamellae: The significance of the exsolution lamellae lies in the timing of their formation with respect to the long and complex metamorphic history of the rock. Following initial crystallisation of the orthoamphibole, subsequent subsolidus unmixing occurred by one or more mechanisms.

Unequivocal evidence of the precise exsolution mechanism is only found in the initial stages of lamellae growth (Smelik and Veblen, 1993) with any subsequent coarsening concealing this early proof. In the case of the feldspars, Smith and Brown (1988) used details of single crystal X-ray diffraction patterns to differentiate between spinodal decomposition and homogeneous nucleation. In the latter mechanism, two distinct sets of diffraction spots are present from inception of lamellae development. In spinodal decomposition spots are first streaked into side bands which transform progressively into dumbbells on maturation, forming distinct pairs only in the final stages of growth.

The broadening of some reflections of the Simiuttat single crystal and the lack of consistent doubling of diffraction spots, might be taken as evidence indicating decomposition of the original orthoamphibole took place below the coherent spinodal. Gittos *et al.* (1976) and Christie and Olsen (1974) argue that coarse, coherent, periodic orthoamphibole exsolution microstructures, which resemble the Simiuttat textures, represent coarsened spinodal decomposition textures. However, Smelik and Veblen (1993) caution that decisive evidence for early stages of spinodal decomposition in orthoamphiboles is generally lacking in coarsened textures such that their full exsolution history can seldom be deduced.

With initial crystallisation of the primary orthoamphibole probably occurring between *c.* 2750 and 2680 Ma, a number of possibilities exist for the timing of lamellae formation. The most likely are: 1. during the latter stages of the same protracted metamorphic episode; 2. during reheating at the time of intrusion of the Qôrqut granite complex *c.* 2550 Ma; 3. under comparatively mild metamorphic conditions in the Proterozoic. The lack of marked coarsening of the lamellae following their initial development, may favour the later date.

Acknowledgements

Dr Ritchie Sims (University of Auckland), Drs Andrew Parker and Lin Sutherland (Australian Museum), Dr Sorena Sorrenson, Mr Jim Collins and Mr Joesph Nelen (Smithsonian Institution), Paul Hoskin (Australian National University), and Dr Peter Bayliss provided expert comment and assistance.

References

Appel, P.W.U. and Jensen, A. (1987) *Gems and Gemology*, 36–42.

Armstrong, J.T. (1988) In: *Microbeam analysis-1988*, pp.239–46, ed. D.E. Newbury. San Francisco Press, San Francisco.

Baadsgaard, H., Lambert, R. St. J and Krupicka, J. (1976) *Geochim. Cosmochim. Acta.*, **40**, 513–27.

Beech, E.M. and Chadwick, B. (1980) *Precamb. Res.*, **11**, 329–55.

Bøggild, O.B. (1905) *Meddelelser om Grønland*, **32**, 1–625.

Bøggild, O.B. (1924) *Det Kongelige Danske Videnskabernes Selskab Mathematiskfysiske Meddelelser*, **6**(3), 1–79.

Christie, O.H.J. and Olsen, A. (1974) *Bull. Soc. Franc. Mineral. Cristallogr.*, **97**, 386–92.

Droop, G.T.R. (1987) *Mineral. Mag.*, **51**, 431–5.

Dymek. R.F. and Smith, M.S. (1990) *Contrib. Mineral. Petrol.*, **105**, 715–30.

Friend, C.R.L., Nutman, A.P., Baadsgaard, H., Kinny P.D. and McGregor V.R. Timing of late Archaean terrane assembly, crustal thickening and granite emplacement in the Nuuk region, southern West Greenland. *Earth Planet. Sci. Lett.* (in press).

Ghose, S. (1981) *Reviews in Mineralogy*, **9A**, 325–72.

Gittos, M.F., Lorimer, G.W. and Champness, P.E. (1976) In *Electron Microscopy in Mineralogy* (H. Wenk, ed.) Springer Verlag, New York. pp.238–47.

Leake, B.E. (1978) *Amer. Mineral.*, **63**, 1023–52.

Maas, R., Kinny, P.D., Williams, I.S., Froude, D.O. and Compston, W. (1992) *Geochim. Cosmochim. Acta*, **56**, 1281–300.

McGregor, V.R. (1993) Geological map of Greenland 1:100,000, Qôrqut 64 V.1 Syd, descriptive text., 40 pp. Copenhagen, Geological Surevy, Greenland.

McGregor, V.R., Nutman, A.P. and Friend, C.R.L. (1986) *LPI Technical Report* **86-04**, 113–69.

McGregor, V.R., Friend, C.R.L. and Nutman, A.P. (1991) *Bull. Geol. Soc. Denmark*, **39**, 179–97.

Milton, D.J. and Ito, J. (1961) *Amer. Mineral.*, **46**, 734–40.

Nutman, A.P., Friend, C.R.L., Baadsgaard, H. and McGregor, V.R. (1989) *Tectonics*, **8**, 573–89.

Pankhurst, R.J., Moorbath, S., Rex., D.C. and Turner, G. (1973) *Earth Planet. Sci. Lett.*, **20**, 157–70.

Parker, A. (1995) *Proc. Roy. Soc. Lond.*, **262**, 349–55.

Robinson, P., Ross, M. and Jaffe, H.W. (1971) *Amer. Mineral.*, **56**, 1005–41.

Robinson, P., Spear, F.S., Schummacher, J.C., Laird, J., Klein, C., Evans, B.W. and Doolan, B.L. (1982) *Reviews in Mineralogy*, **9B**, 1–228.

Seki, Y. and Yamasaki, M. (1957) *Amer. Mineral.*, **42**, 506–20.

Smelik, E.A. and Veblen, D.R. (1993) *Amer. Mineral.*, **78**, 511–32.

Smith, J.V. and Brown, W.L. (1988) *Feldspar Minerals*. Springer-Verlag, Berlin.

Smith, M.S., Dymek, R.F. and Chadwick, B. (1992) *Precambrian Res.*, **57**, 49–90.

Treloar, P.J. and Putnis, A. (1982) *Mineral. Mag.*, **45**, 55–62.

Williams I.S. and Claesson, S. (1987) *Contrib. Mineral. Petrol.*, **97**, 205–17.

[*Manuscript received 5 February 1996: revised 13 May 1996*].